Investigation of the Polymorphs of Dimethyl-3,6-Dichloro-2,5-Dihydroxyterephthalate by ^{13}C Solid-State NMR Spectroscopy

Mark Strohmeier,[†] Anita M. Orendt,[‡] D. W. Alderman,[†] and David M. Grant*[,†]

Contribution from the Department of Chemistry, University of Utah, 315 South 1400 East, Salt Lake City, Utah 84112-0850, and Center for High Performance Computing, University of Utah, 155 South 1452 East, Salt Lake City, Utah 84112-0190

Received October 5, 2000. Revised Manuscript Received December 12, 2000

Abstract: Two of the three conformational polymorphs of dimethyl-3,6-dichloro-2,5-dihydroxyterephthalate are studied by solid-state NMR techniques. The structural differences between the polymorphs have previously been studied by X-ray. In these two polymorphs named white and yellow due to their color, the major structural difference is the torsional angle between the ester group and the aromatic ring. The yellow form has a dihedral angle of 4° between the plane of the aromatic ring and the plane of the ester group, while the white form has two different molecules per unit cell with dihedral angles of 70° and 85°. This change greatly affects the conjugation in the π-electronic system. In addition, there are differences in the hydrogen-bonding patterns, with the white form having intermolecular hydrogen bonds and the yellow form having intramolecular hydrogen bonds. In this work, the carbon isotropic chemical shift values and the chlorine electric field gradient (EFG) tensor information are extracted from the ^{13}C MAS spectra, and the principal values of the chemical shift tensors of the carbons are obtained from 2D FIREMAT experiments. Quantum chemical calculations of the chemical shift tensor data as well as the EFG tensor are performed at the HF and DFT levels of theory on individual molecules and on stacks of three molecules to account for the important intermolecular interactions in the white form. The differences between the spectral data on the two polymorphs are discussed in terms of the known electronic and structural differences.

Introduction

Due to the conformational flexibility of organic molecules distinct crystal structures can often be obtained by varying crystallization conditions. This phenomenon is known as polymorphism. Conformational polymorphism, as encountered in dimethyl-3,6-dichloro-2,5-dihydroxyterephthalate (Scheme 1), is one of several categories of polymorphism. The analysis of polymorphs is increasingly important in pharmaceutics, material science, and industrial chemistry because solubility, color, and mechanical properties in solids depend inherently on the crystal structure and the conformation of the molecule in a given polymorph.[1,2]

Solid-state NMR is known to be a powerful method to investigate the effects of differences in conformation and packing without the limitations of diffraction methods. Chemical shifts, especially, are very sensitive to local conformations. Most previous solid-state NMR investigations of polymorphs have relied on differences in isotropic chemical shifts.[3−11] Only a few studies have utilized the chemical shift principal values to investigate polymorphism.[12,13] However, the chemical shift is a second rank tensor and contains detailed orientational information. Thus, the principal values and the orientations of the chemical shift tensor may reveal a deeper insight into the conformation of the compound. The full tensor is only accessible by single crystal studies, but from measurements on powdered samples the chemical shift principal values may be obtained.

Scheme 1

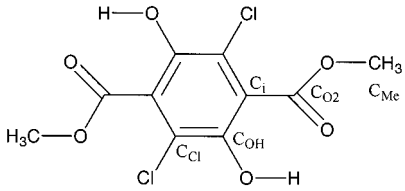

* To whom the correspondence should be addressed.
[†] Department of Chemistry, University of Utah
[‡] Center for High Performance Computing, University of Utah

(1) Threlfall, T. L. *Analyst* **1995**, *120*, 2435.
(2) Byrn, S. R.; Pfeiffer, R. R.; Stephenson, G.; Grant, D. J. W.; Gleason, W. B. *Chem. Mater.* **1994**, *6*, 1148.
(3) Anwar, J.; Tarling, S. E.; Barnes, P. *J. Pharm. Sci.* **1989**, *78*, **4**, 337.
(4) Kimura, K.; Hirayama, F.; Uekama, K. *J. Pharm. Sci*, **1999**, *88*, **4**, 385.
(5) Stockton, G. W.; Godfrey, R.; Hitchcock, P.; Mendelsohn, R.; Mowery, P. C.; Rajan, S.; Walker, A. F. *J. Chem. Soc., Perkin Trans. 2* **1998**, *9*, 2061.
(6) Schmidt, A.; Kababya, S.; Appel, M.; Khatib, S.; Botoshansky, M.; Eichen, Y. *J. Am. Chem. Soc.* **1999**, *121* 11291.
(7) Singh, D.; Marshall, P. V.; Shields, L.; York, P. *J. Pharm. Sci.* **1998**, *87*, **5**, 655.
(8) Harris, R. K.; Kenwright, A. M.; Say, B. J.; Yeung, R. R.; Fletton, R. A.; Lancaster, R. W.; Hardgrove, G. L., Jr. *Spectrochim. Acta* **1990**, *46A*, 927.
(9) Fletton, R. A.; Harris, R. K.; Kenwright, A. M.; Lancaster, R. W.; Packer, K. J.; Sheppard, N. *Spectrochim. Acta* **1987**, *43A*, 1111.
(10) Harris, R. K.; Yeung, R. R.; Lamont, R. B.; Lancaster, R. W.; Lynn, S. M.; Staniforth, S. E. *J. Chem. Soc., Perkin Trans. 2* **1997**, *8*, 2653.
(11) Zell, M. T.; Padden, B. E.; Grant, D. J. W.; Chapeau, M.-C.; Prakash, I.; Munson, E. J. *J. Am. Chem. Soc.* **1999**, *121*, 1372.
(12) Smith, J.; MacNamara, E.; Raftery, D.; Borchardt, T.; Byrn, S. *J. Am. Chem. Soc.* **1998**, *120*, 11710.
(13) Christopher, E. A.; Harris, R. K.; Fletton, R. A. *Solid State Nucl. Magn. Reson.* **1992**, *1*, 93.

10.1021/ja003599b CCC: $20.00
Published on Web 02/02/2001

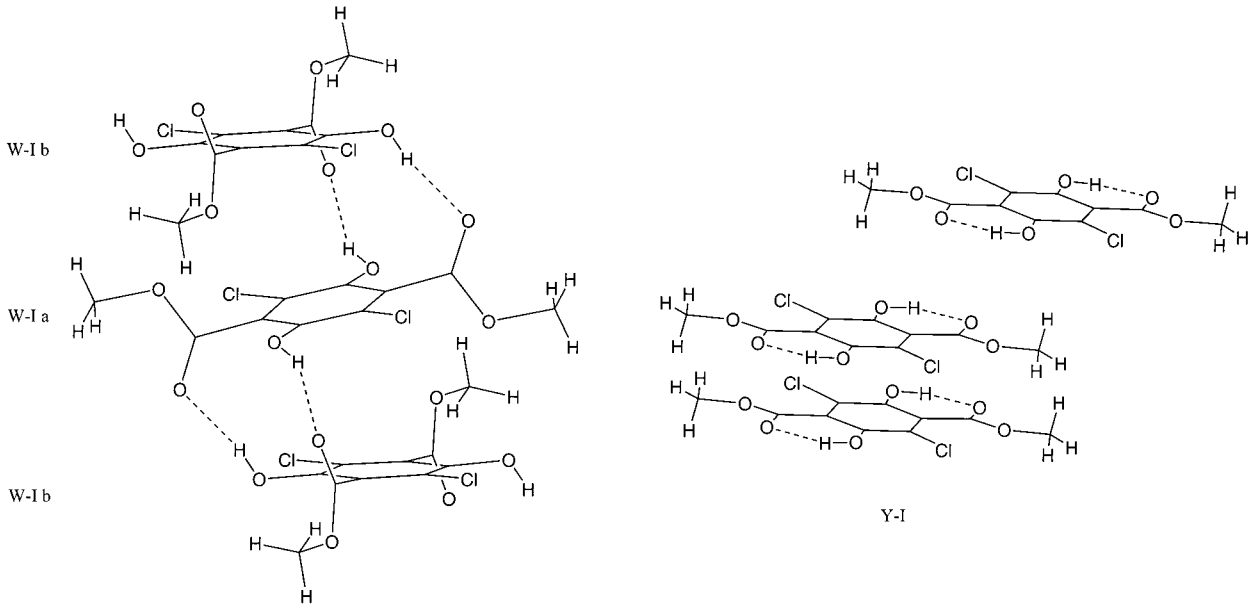

Figure 1. View of the molecule stacks chosen for the calculations on **W-I a** and **Y-I**, The stack used for the **W-I b** stack of three molecules has the same configuration as the one for **W-I a**, but with the **W-I b** molecules sandwiched between two **W-I a** molecules.

The recently developed 2D FIREMAT[14] technique with TIGER[15] processing is one such method which makes it possible to obtain the chemical shift principal values for each resolved isotropic chemical shift from a powdered sample.

Another probe that is sensitive to conformation is the quadrupolar coupling of nuclei with a quadrupole moment. The magnitude of the coupling depends on the size of the quadrupole moment of the nucleus and the size and orientation of the electromagnetic field gradient (EFG) at the nucleus. The EFG is generated by the electron distribution around the nucleus and is therefore very sensitive to changes in the electronic environment caused by variations in conformation and packing in the crystal. The quadrupolar coupling is described by a traceless second rank tensor. It may be observed in solid-state MAS NMR spectra of common spin $^1/_2$ nuclei as a dipolar coupling between the quadrupolar nucleus (^{35}Cl and ^{37}Cl) and the observed spin $^1/_2$ nucleus (^{13}C), which is not completely averaged by magic angle spinning.[16] Simulation of the resulting Pake doublet-like resonance in the MAS spectrum allows the determination of most parts of the EFG-tensor and the internuclear distance.[16−19]

In this paper solid-state NMR is used to investigate the conformational polymorphism of dimethyl-3,6-dichloro-2,5-dihydroxyterephthalate (**I**). The polymorphism of **I** was discovered by Hantzsch[20] over 100 years ago and has attracted the attention of many researchers. **I** forms three different conformational polymorphs, which are named by their color: yellow (**Y-I**), light yellow (**LY-I**) and white (**W-I**). All three forms are stable at room temperature and can be stored for years without phase transition. Byrn et al.[21,22] solved the crystal structure of **W-I** and **Y-I**, investigated the phase transition from **Y-I** to **W-I** at 385−410 K with optical microscopy and differential scanning calorimetry, and reported the ^{35}Cl NQR frequencies. The most striking difference between **W-I** and **Y-I** is the torsional angle between the planar aromatic system and the ester group, resulting in different crystal packing and a change in hydrogen bonding between the carbonyl and the hydroxy group in the molecule. The torsional angle in **Y-I** is 4° and an intramolecular hydrogen bond exists. Due to this low torsional angle the substituent sphere is sterically crowded resulting in longer C−Cl bonds and distorted bond angles. **Y-I** has one $^1/_2$ centrosymmetric molecule per asymmetric cell, whereas **W-I** has two $^1/_2$ centrosymmetric molecules per asymmetric cell, with torsional angles of 70° (**W-I a**) and 85° (**W-I b**) in these molecules, respectively. In addition, there is intermolecular hydrogen bonding in **W-I** (Figure 1). The large torsional angle in **W-I** has an extensive impact on the overall electronic structure of the compound, since the $\pi-\pi$ overlap between the carbonyl group and the aromatic system is negligible compared to that in **Y-I** where the low torsional angle allows appreciable $\pi-\pi$ overlap. Swiatkiewicz et al.[23] assigned the solid-state Raman and electronic photoexcitation and emission spectra for **W-I** and **Y-I** and used these methods to investigate the phase transition at 380−400 K.

LY-I was discovered by Yang et al.,[24] who determined that it has a torsional angle of 40° and crystal packing similar to **Y-I**. They performed a variable-temperature single-crystal X-ray diffraction study and a combined optical microscopy and differential scanning calorimetry study to investigate the connection between internal molecular motion and conformational isomerization between the different polymorphic forms.[25] These studies reveal a large temperature dependence of the torsional angle of the ester group with respect to the aromatic plane. They also found large anisotropic displacement parameters for **Y-I**

(14) Alderman, D. W.; McGeorge, G.; Hu, J. Z.; Pugmire, R. J.; Grant, D. M. *Mol. Phys.* **1998**, *95*, **6**, 1113.
(15) McGeorge, G.; Hu, J. Z.; Mayne, C. L.; Alderman, D. W.; Pugmire, R. J.; Grant, D. M. *J. Magn. Reson.* **1997**, *129*, 134.
(16) Menger, E. M.; Veeman, W. S. *J. Magn. Reson.* **1982**, *46*, 257.
(17) Olivieri, A. C.; Elguero, J.; Sobrados, I.; Cabildo, P.; Claramunt, R. M. *J. Phys. Chem.* **1994**, *98*, 5207.
(18) Eichele, K.; Wasylischen, R. E.; Grossert, J. S.; Olivieri, A. C. *J. Phys. Chem.* **1995**, *99*, 10110.
(19) Alacoron, S. H.; Olivieri, A. C.; Carss, S. A.; Harris, R. K.; Zuriaga, M. J.; Monti, G. A. *J. Magn. Reson., Ser A* **1995**, *116*, 244.
(20) Hantzsch, A. *Chem. Ber.* **1915**, *48*, 785.
(21) Byrn, S. R.; Curtin, D. Y.; Paul, I. C. *J. Am. Chem. Soc.* **1971**, *94*, 890.
(22) Curtin, D. Y.; Byrn, S. R. *J. Am. Chem. Soc.* **1969**, *91*, 1865.
(23) Swiatkiewicz, J.; Prasad, P. N. *J. Am. Chem. Soc.* **1982**, *104*, 6913.
(24) Yang, Q.-C.; Richardson, M. F.; Dunitz, J. D. *Acta Crystallogr.* **1989**, *B45*, 312.
(25) Richardson, M. F.; Yang, Q.-C.; Novotny-Bregger, E.; Dunitz, J. D. *Acta Crystallogr.* **1990**, *B46*, 653.

compared to the other two forms and proposed a mechanism for the thermal phase transition.[24]

In this work the ^{13}C CPMAS spectra at 2.35, 4.7, and 9.4 T and the FIREMAT spectra at 9.4 T are obtained on both **Y-I** and **W-I**. From simulations of the ^{13}C CPMAS spectra, dipolar information as well as information on the EFG tensor are obtained. The FIREMAT datasets provide the chemical shift principal values of all carbon positions of the two polymorphic forms. The chemical shift principal values and the EFG tensors are calculated for the known low-temperature structures using HF and DFT methods. To account for intermolecular interactions these calculations are done on isolated molecules and on stacks of three molecules. The theoretical values are compared to experiment.

Experimental Section

Sample Preparation. Dicarbomethoxy-1,4-cyclohexanedione was purchased from Arcos and used without further purification. HPLC-grade methanol and benzene were stored over 4 Å molecular sieves and used for recrystallization.

Dimethyl 2−5-Dichloro 3,6 dihydroxyterephthalate (I). Dicarbomethoxy-1,4-cyclohexanedione (3.6 g, 15.3 mmol) was dissolved in 60 mL of acetic acid (reagent grade), and chlorine was bubbled through this solution for 1.5 h. It was then heated to 75 °C and stirred overnight. Since the cyclohexadione shows blue while **I** shows green fluorescence, the reaction progress can easily be monitored by TLC on silica with benzene eluent. After completion of the reaction the solvent was removed to precipitate a yellow solid (2.55 g). This crude product was further purified on a column packed with silica gel (200−400 mesh) with benzene eluent. The overall yield of **I** was 0.96 g (22%).

EI-MS [*m*/*z* (%)]: 293.9 (M^+, 24.3), 261.9 ($\Delta = 32$, $-CH_3OH$, 91.2), 229.9 ($\Delta = 64$, -2 (CH_3OH), 100), 201.9 ($\Delta = 92$, -2 (CH_3OH) $-CO$, 23.8)

^{13}C NMR (500 MHZ, methanol): δ (ppm) = 53.46 (C_{Me}), 119.40 (C_{Cl}), 126.18 (C_i), 145.92 (C_{OH}), 166.93 (C_{O2}).

Crystallization. The two different polymorphs studied were obtained by recrystallization from different solvents by slowly cooling a saturated refluxing solution of **I**. If the solution was not refluxed for several minutes, a mixture of different polymorphic forms was usually obtained. White needles are preferentially formed from a benzene solution, but occasionally the formation of yellow plates is observed. In this case the solution is reheated and refluxed for several minutes to remove all yellow seed crystals from the system.

Y-I crystallizes preferentially from saturated methanol solutions. If the white needles appear along with the yellow plates, the solution is heated again to dissolve the crystals. Since **W-I** is more soluble in methanol, the yellow crystals remain and become effective seeds. The obtained crystals were then filtered off, washed, and dried in a vacuum to remove residual solvent.

X-ray Powder Diffraction. The X-ray powder diffraction patterns of the two polymorphic forms were recorded on a Rigaku diffractometer with monochromated Cu Kα radiation ($\lambda = 1.540598$ Å). Data were collected between a 2θ angle of 5° and 60° in a step scan mode with 0.05° steps and a collection time of 0.3 s. Approximately 20 mg of sample was cautiously ground, placed on a greased microscope slide, and carefully smoothed with a spatula.

The theoretical XRD patterns based on the room-temperature X-ray single-crystal data[21,24] were calculated using the Molecular Simulations Inc. software package and compared to the collected data to confirm the crystal form of the sample.

Solid-State Spectroscopy. The solid-state CPMAS spectra at 2.35 T were recorded on a Chemagnetics CMX100 spectrometer equipped with a 7.5 mm Chemagnetics high-speed-spinning PENCIL probe with a ^{13}C frequency of 25.152 MHz. The CPMAS spectra at 4.7 T were recorded on a Varian VXR-200 spectrometer using a 5 mm high-speed-spinning probe from Doty Scientific Inc. at a ^{13}C frequency of 50.318 MHz. The high-resolution spectra at 9.4 T were collected on a Chemagnetics CMX400 spectrometer equipped with a 7.5 mm Chemagnetics high-speed-spinning PENCIL probe at a ^{13}C frequency of 100.625 MHz. On the 400 MHz spectrometer TOSS[26] sideband suppression and TPPM[27,28] decoupling with a phase angle of 16° was used. The ^{1}H T_1 was measured to be 33 s for **Y-I** and 13 s for **W-I** at 100.625 MHz.

The following optimized experimental conditions were used: a 7 ms contact time and a 12 s recycle time for **W-I** and a 9 ms contact time and 33 s recycle time for **Y-I**. The proton 90° pulse was approximately 4.1 μs on all three spectrometer systems.

The ^{13}C FIREMAT[14] experiments were performed on the CMX400, using the 7.5 mm probe with a feedback circuit to synchronize the pulse sequence to the rotor position. The 5π pulse sequence[29] was used with TPPM decoupling using a phase angle of 36°. For **W-I** the spectra window in the acquisition dimension was 78.125 kHz, the spectral width in the evolution dimension was 13 kHz, and the spinning speed was 812.5 Hz. For **Y-I** the spectra width in the acquisition dimension was 63.291 kHz, in the evolution dimension it was 10.504 kHz, and a spinning speed of 659 Hz was used. For both forms 16 complex increments were taken with 384 scans each.

The 2D data were processed on a Sun Enterprise 3500. Individual spinning side-band patterns were obtained from the 2D dataset using TIGER[15] processing. TIGER processing requires a linear model for the evolution dimension, which is obtained by fitting a guide spectrum with Gaussian and Lorentzian line shapes. The line shapes encountered in the 9.4 T spectra are well described by Gaussian and Lorentzian line shapes, despite the pattern-like nature of the coupled shifts. The model is then used to extract individual sideband patterns at the maximum intensity for the different isotropic shifts.

All sideband patterns were fit with a single CSA sideband pattern model; only when breakthrough from a nearby resonance was apparent in the spectrum was a second or third sideband pattern included in the model to obtain the best fit. The principal shift values of this additional sideband patterns were taken from the best fits of the neighboring resonances, and only their intensities were optimized.

The residual dipolar coupling apparent in the sideband manifold was not incorporated into the sideband model. The effect of the residual dipolar coupling resulting from quadrupolar interactions onto the shape of the sidebands is well understood.[30] The effect on the FIREMAT spectrum, however, is more complicated and was not previously investigated. A challenging problem arises from the large number of parameters that must be considered in a complete description of the dipolar-coupled sideband pattern since both Cl isotopes interact with the ^{13}C nuclei. Thus, it is only possible to fit the coupled sideband pattern when both the chemical shift anisotropy, the ^{13}C$-^{35,37}$Cl dipolar coupling constants and the ^{35,37}Cl quadrupolar couplings are combined in the computation of the line patterns.

Theory of Residual ^{35,37}Cl$-^{13}$C Dipolar Couplings and MAS Simulations. Since the ratio of the quadrupolar coupling χ to the Larmor frequency ν is larger than 1 for both ^{35}Cl and ^{37}Cl at commonly used field strengths in solid-state NMR, first-order perturbation is not applicable to describe the effect of the quadrupolar Hamiltonian. The total Hamiltonian for an *I*,*S* spin system where *I* is spin $^1/_2$ (C) and *S* is spin $^3/_2$ (Cl) is given by

$$H^{\text{total}} = H^{\text{IZ}} + H^{\text{SZ}} + H^{\text{SQ}} + H^{\text{D}} + H^{\text{J}}$$

Applying first-order perturbation to the coupling Hamiltonian, only the combined Zeeman and quadrupolar Hamiltonian have to be diagonalized.

$$H^0 = H^{\text{IZ}} + H^{\text{SZ}} + H^{\text{SQ}} \quad H' = H^{\text{D}} + H^{\text{J}}$$

Using the EFG principal axis system as the axis system with the magnetic field direction specified by α and β (Figure 2), the complete

(26) Geen, H.; Bodenhausen, G. *J. Am. Chem. Soc.* **1993**, *115*, 1579.
(27) Bennet, A. E.; Rienstra, C. M.; Auger, M.; Lakshmi, K. V. *J. Chem. Phys.* **1995**, *103*, 6951.
(28) McGeorge, G.; Alderman, D. W.; Grant, D. M. *J. Magn. Reson.* **1999**, *137*, 138.
(29) Hu, J. Z.; Alderman, D. W.; Ye, C.; Pugmuire, R. J.; Grant, D. M. *J. Magn. Reson.* A, **1993**, *105*, 82.
(30) Zheng, Z.; Gan, Z.; Sethi, N. K.; Alderman, D. W.; Grant, D. M. *J. Magn. Reson.* **1991**, *95*, 509.

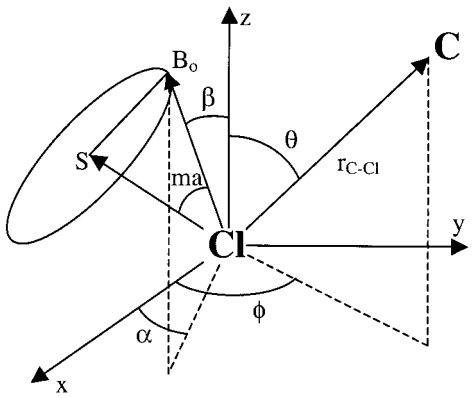

Figure 2. Relationship between the C−Cl bond vector, the spinning axis *S* and the magnetic field B_o in the EFG principal axis system. The angles θ and ϕ specify the orientation of the internuclear vector, and the angles α and β specify the orientation of the magnetic field vector in the EFG principal axis system, respectively. The magic angle is abbreviated by ma.

quadrupolar Hamiltonian[31] is given by:

$$H^{SQ} = \frac{e^2Q}{4S(2S-1)} \cdot q_0 \cdot [(3\hat{S}_X^2 - \hat{S}^2) + \eta(\hat{S}_X^2 + \hat{S}_Y^2)]$$

Diagonalizing the combined quadrupolar and Zeeman Hamiltonian yields the wave function as an expansion of Zeeman *IS* eigenstates.

$$\Psi^o_{mn}(\alpha,\beta) = \sum_{-I}^{I}\sum_{-S}^{S} a_m(\alpha,\beta)a_n(\alpha,\beta)|\Phi_m\rangle|\Phi_n\rangle$$

Once all $a_m(\alpha,\beta)$ and $a_n(\alpha,\beta)$ coefficients are determined, the combined dipolar and scalar *I*,*S* coupling terms may be calculated numerically. For the sake of simplicity, the same principal axis system is assumed for the dipolar and scalar coupling. The ^{35,37}Cl-coupled ^{13}C resonance is then calculated by:

$$\Delta\nu_{1/2n}(\alpha,\beta) = \langle\Psi^o_{-1/2n}(\alpha,\beta)|H'|\Psi^o_{-1/2n}(\alpha,\beta)\rangle - \langle\Psi^o_{1/2n}(\alpha,\beta)|H'|\Psi^o_{1/2n}(\alpha,\beta)\rangle$$

The powder average is obtained by collecting the resonance frequencies for all α and β; the MAS line shapes can then be obtained by averaging over the magic angle.

In this approach no assumptions regarding the symmetry and the orientation of the EFG tensor are made. The common assumption of an axially symmetric EFG tensor for chlorine is applicable for most cases, but as soon as the axial symmetry of the three free-electron pairs on chlorine is broken, the asymmetry

$$\eta = (q_{xx} - q_{yy})/q_{zz}$$

becomes appreciable different from 0. That is the case when chlorine is attached to a sp^2 hybridized carbon atom with an electron deficiency in the p-orbital, resulting in a polarization of the chlorine lone pairs parallel to the electron-deficient p-orbital. In these cases asymmetries as high as 0.26 are observed.[32]

Since no assumptions regarding the symmetry and orientation of the EFG tensor are made, it is possible to obtain not only its magnitude and asymmetry but also its orientation with respect to the molecular frame even when the tensor is not axially symmetric. To be able to retrieve this information it is necessary that the unique axis is not parallel to the unique dipolar coupling axis, that is, internuclear vector ($\theta \neq 0$). In the investigated compound the ^{35,37}Cl is coupled to three neighboring ^{13}C where the unique EFG tensor axis is directed along the C−Cl bond as generally found. This configuration makes it possible to retrieve the orientational information from the coupling of ^{35,37}Cl to the carbons in β-position (Figure 2).

The ^{35,37}Cl-coupled ^{13}C line shapes were calculated by diagonalizing the appropriate Hamiltonian and applying the calculated wave functions on H' using software written in Fortran 77. Different spinning-axis orientations were produced using the POWDER[33] approach, and the MAS line shapes were then calculated by averaging over the magic angle. It was found that 47 steps per rotation cycle and 4096 crystal orientations were sufficient to obtain all expected line shape features in the simulation. The program was tested and found to produce simulations in good agreement with simulations and MAS spectra from the literature.[17−19] The calculations for a ^{35,37}Cl−^{13}C spin-pair required about 1 min on a Sun Enterprise 3500.

The quadrupolar coupling constants previously found in NQR experiments[21] were used in the simulations. However, an average value for the two molecules per asymmetric cell was used to simplify the simulations for **W-I**. The small difference between the two coupling constants and the good agreement between simulation and experimental spectra show that this assumption is correct within the experimental resolution. The asymmetry used in the simulations was systematically improved, starting from values found for similar compounds.[32] Initial values for the dipolar coupling constants for the different forms were calculated using the C−Cl distances found in the room-temperature crystal structure.[21] Care was taken that the geometrical restraint imposed by the molecular geometry onto the four-body system was conserved when the spatial orientation of the three internuclear vectors with respect to the EFG principal axis system was determined (Figure 2). Since the MAS spectra of **W-I** is relatively insensitive to *J* coupling due to overlap with the C_i resonance, the same scalar coupling found in **Y-I** was also assumed for **W-I**. The same EFG-tensor parameters were used for all three different field strengths. The resulting spectra were then line-broadened using a Gaussian function and compared to the collected data. Agreement was judged to be excellent by visual inspection, as can be seen in Figures 3 and 4 for **Y-I** and **W-I**, respectively.

Quantum Mechanical Calculations. DFT (density functional theory) and HF (Hartree−Fock) calculations were performed with the Gaussian 98 computer program[34] using the GIAO[35] (gauge invariant atomic orbitals) method and the D95** basis set.[36] The DFT calculations use the B3LYP[37,38,39] exchange correlation functional. The shift tensor calculations were done on isolated molecules as well as on stacks of three molecules to account for intermolecular interactions using the known low-temperature structures.[24] The C−H bond distances were lengthened to 1.085 Å as C−H distances found by X-ray diffraction are known to be too short. As the chemical shift is known to be very sensitive to the geometry, in particular the C−H bond lengths, the standard procedure has often been to optimize all proton positions.[40] However, in this case due to the size of the system (76 atoms) it was

(31) Slichter, C. P. *Principles of Magnetic Resonance*, 3rd ed.; Springer: New York 1996; p 496.

(32) Lucken E. A. C. *Nuclear Quadrupole Coupling Constants*; Academic Press: New York 1969; p 167.

(33) Alderman, D. W.; Solum, M. S.; Grant, D. W. *J. Chem. Phys.* **1986**, *84*, **7**, 3717.

(34) Frisch, M. J.; Trucks, G. W.; Schlegel, H. B.; Scuseria, G. E.; Robb, M. A.; Cheeseman, J. R.; Zakrzewski, V. G.; Montgomery, J. A., Jr.; Stratmann, R. E.; Burant, J. C.; Dapprich, S.; Millam, J. M.; Daniels, A. D.; Kudin, K. N.; Strain, M. C.; Farkas, O.; Tomasi, J.; Barone, V.; Cossi, M.; Cammi, R.; Mennucci, B.; Pomelli, C.; Adamo, C.; Clifford, S.; Ochterski, J.; Petersson, G. A.; Ayala, P. Y.; Cui, Q.; Morokuma, K.; Malick, D. K.; Rabuck, A. D.; Raghavachari, K.; Foresman, J. B.; Cioslowski, J.; Ortiz, J. V.; Baboul, A. G.; Stefanov, B. B.; Liu, G.; Liashenko, A.; Piskorz, P.; Komaromi, I.; Gomperts, R.; Martin, R. L.; Fox, D. J.; Keith, T.; Al-Laham, M. A.; Peng, C. Y.; Nanayakkara, A.; Gonzalez, C.; Challacombe, M.; Gill, P. M. W.; Johnson, B.; Chen, W.; Wong, M. W.; Andres, J. L.; Gonzalez, C.; Head-Gordon, M.; Replogle, E. S.; Pople J. A. *Gaussian 98*, revision A.7; Gaussian, Inc.: Pittsburgh, PA, 1998.

(35) Ditchfield, R. *Mol. Phys.* **1974**, *27*, 789.

(36) Dunning, T. H., Jr.; Hay, P. J. In *Modern Theoretical Chemistry*; Schaefer, H. F., III, Ed.; Plenum: New York, 1976; pp 1−28.

(37) Becke, A. D. *J. Chem. Phys.* **1993**, *98*, 5648.

(38) Lee, C.; Yang, W.; Parr, R. G. *Phys. Rev. B* **1988**, *37*, 785.

(39) Miehlich, B.; Savin, A.; Stoll, H.; Preuss, H. *Chem. Phys. Lett.* **1989**, *157*, 200.

(40) Liu, F.: Phung, C. G.; Alderman, D. W.; Grant, D. M. *J. Am. Chem. Soc.* **1996**, *118*, 10629.

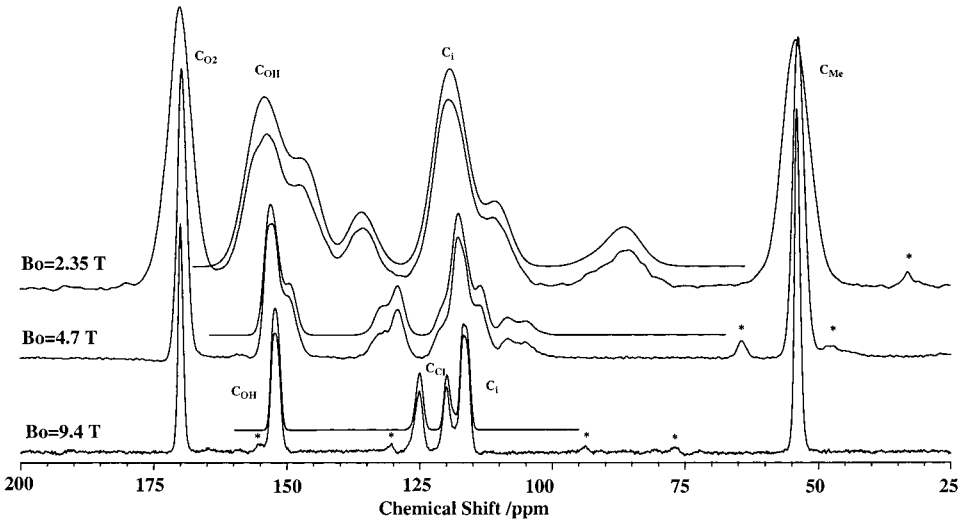

Figure 3. ^{13}C CPMAS spectra of **Y-I** and simulations of the coupled ^{13}C resonances at 2.35, 4.7, and 9.4 T. Spinning sidebands are marked by asterisks.

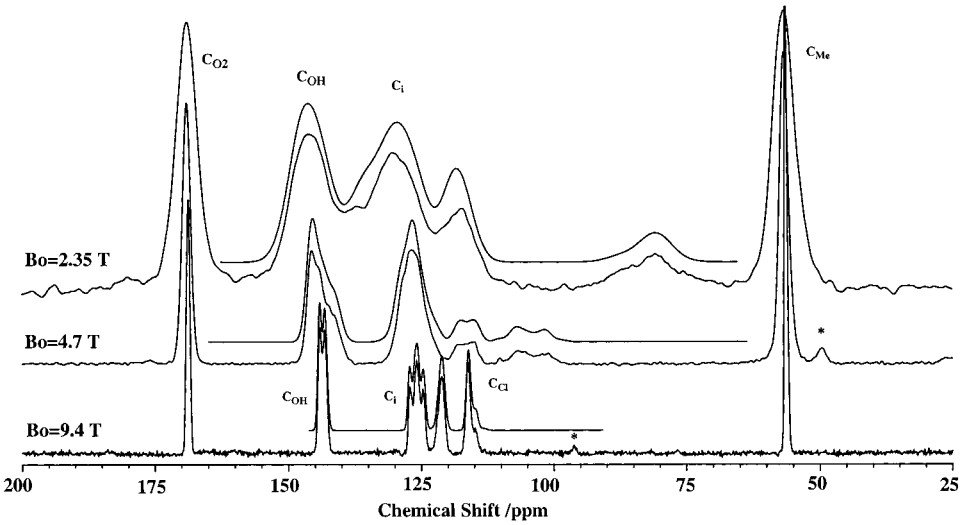

Figure 4. ^{13}C CPMAS spectra of **W-I** and simulations of the coupled ^{13}C resonances at 2.35, 4.7, and 9.4 T. Spinning sidebands are marked by asterisks.

felt sufficient to adjust all C−H bond lengths to a single value. The structures used for stacks of three molecules are shown in Figure 1. Since the inversion symmetry of the system is broken when calculations are performed on the stack chosen for **Y-I**, only the half of the molecule that is exposed to the intermolecular interactions is considered. The shielding values were converted to the ppm scale by using the slope and intercept of the least-squares fit of the correlation between experimental data and the calculated shielding values.

The electrostatic field properties were calculated using the same self-consistent field wave functions employed for the NMR calculations. The EFG values were converted to the nuclear coupling constant for ^{35}Cl in frequency units by:

$$\chi_{ZZ} = \frac{e^2 Q \cdot q_{ZZ}}{h}$$

With a quadrupole moment for ^{35}Cl of $Q = -0.08165 \times 10^{-28}$ Q/m^2, a conversion factor of 1 au $= -19.184484$ MHz is obtained.[41]

Results and Discussion

For the purpose of the following discussion the nomenclature shown in Scheme 1 is used. The CPMAS spectra of **W-I** and **Y-I** at different fields are shown in Figures 3 and 4, respectively. The chemical shift data obtained from the simulations of the residual dipolar coupling and the FIREMAT experiment along with solution isotropic chemical shifts obtained in different solvents are given in Table 1. The parameters used for the simulations of the CPMAS spectra are given in Tables 2 and 3.

Assignment of the ^{13}C CPMAS Spectra. Previously described features[17] of ^{13}C MAS spectral patterns of carbons coupled to $^{35,37}Cl$ are observed for the carbons in α (C_{Cl}) and β (C_{OH} and C_i) positions relative to chlorine. While the spectra obtained at 4.7 and 2.35 T show the dominating effect of the $^{13}C-^{35,37}Cl$ residual dipolar coupling, the simpler spectra obtained at 9.4 T provides directly assignable resonances. At 9.4 T the strong coupling to the $^{35,37}Cl$ at the C_{Cl} position results in a doublet-like resonance in both forms with a splitting of approximately 500 Hz. The aromatic C_{OH} resonance is found at lower field in the aromatic shift region than the C_i resonance for both polymorphic forms. The C_{OH} and C_i resonances also show the effect of the residual coupling but with a smaller coupling as a result of the larger distance and a different

(41) Pyykko, P. *Z. Naturforsch.* **1992**, *47a*, 189.

Table 1. Experimental Chemical Shift Tensor Principal Values for **W-I** and **Y-I**/ppm

	δ_{11}	δ_{22}	δ_{33}	δ_{iso}	δ_{CPMAS}	δ_{MeOD}	δ_{DMSO}	δ_{CDCl3}	δ_{C6D6}
					C_{O2}				
W-I	260.4	138.3	108.4	169.0	168.5[a]	166.9	164.3		
Y-I	251.1	149.4	110.0	170.2	169.8			167.5	167.8
					C_{OH}				
W-I	213.9	157.5	60.0	143.9	143.6[a]	145.9	143.4		
Y-I	224.3	171.2	61.5	152.3	152.1			148.3	149.3
					C_{Cl}				
W−I	189.8	118.6	47.9	118.8	118.5[a]	119.4	117.9		
Y−I	183.9	127.4	56.4	122.6	122.3[a]			119.6	120.3
					C_i [b]				
W−I a	189.5	144.9	41.7	125.4	125.1[a]	126.2	125.7		
W−I b	191.4	146.0	42.9	126.8	126.7[a]				
Y−I	177.8	142.6	28.4	116.3	116.4			119.3	119.8
					C_{Me}				
W−I	86.2	69.1	13.9	56.4	56.3	53.5	52.9		
Y−I	83.8	66.5	10.6	53.6	54.1			53.4	52.9

[a] The isotropic chemical shift is determined by simulating the CPMAS spectra. [b] The two molecules per asymmetric cell in the white form are resolved for the C_i position

Table 2. Coupling Parameters Used in the CPMAS Spectral Simulations

	D /Hz			*J* /Hz
	C_{Cl}	C_i	C_{OH}	
W-I	559	147	150	−20
Y-I	549	137	156	−20

Table 3. Calculated and Experimental Quadrupolar Coupling Constants for ^{35}Cl and Orientations

	χ_{zz} MHz	χ_{xx} MHz	χ_{yy} MHz	η	θC_{Cl} deg	ϕC_I [a] deg	ϕC_{OH} [a] deg
			experiment				
W-I	−70.65[b]	−	−	0.04	0	90[c]	90[c]
Y-I	−73.30[b]	−	−	0.15	0	90	90
			B3LYP D95**				
W-I a	−71.32	33.54	37.63	0.06	0	−119	71
W-I b	−69.92	30.91	37.86	0.07	0	−108	74
Y-I	−76.06	29.24	46.82	0.23	0	−91	89
			B3LYP D95** Three Molecules				
W-I a	−71.92	33.34	38.57	0.07	0	−101	82
W-I b	−71.56	33.28	38.29	0.08	1	−95	87
Y-I	−76.41	29.12	47.3	0.24	1	−92	88
			HF D95**				
W-I a	−74.11	35.44	38.67	0.04	0	−122	61
W-I b	−74.39	35.67	38.72	0.04	0	−108	74
Y-I	−79.95	32.35	47.6	0.19	1	−91	89
			HF D95** Three Molecules				
W-I a	−74.92	35.76	39.14	0.05	0	−107	75
W-I b	−74.13	35.33	38.8	0.05	0	−97	85
Y-I	−80.53	32.4	48.13	0.20	1	−92	89

[a] Because of the inversion symmetry of the EFG tensor, the residual dipolar coupling observed in the CPMAS spectra is independent of the sign. [b] Taken from ref 22. [c] The angle ϕ has only a small effect on the simulation because of the small asymmetry η.

interaction angle in the EFG principal axis system between the nuclei. In the case of **Y-I** the couplings between the ^{35,37}Cl and the C_{OH} and C_i position result in broadened resonances at 9.4 T. For **W-I** distorted doublet and triplet resonances are observed for C_{OH} and C_i, respectively. Simulations of the residual coupling in **W-I** reveal that doublet resonances are expected for these two positions at 9.4 T. The triplet resonance for C_i is best explained by two overlapping doublets resulting from the two C_i of the two molecules per asymmetric cell having an isotropic shift difference of $\Delta\delta = 1.6$ ppm. The excellent agreement between simulation and experimental CPMAS spectra indicate that the two molecules per asymmetric cell are indeed resolved for the C_i position.

At 4.7 T field strength the ^{35,37}Cl quadrupolar interaction is stronger than the Zeeman interaction, and the expected triplet pattern with a 2:1:1 intensity ratio is observed for the C_{Cl} position in both spectra. Due to overlap with the C_i resonance only two peaks are resolved in either spectrum. The C_i and C_{OH} resonance are broadened, and shoulders are formed by the residual coupling at this field. At 2.35 T the chlorine is predominately quantized by the quadrupolar interaction, and four patterns result for C_{Cl} from the residual coupling, each corresponding to a chlorine eigenstate. The extensive overlap in the broadened C_i and C_{OH} resonances makes it difficult to recognize individual features of the overlapping peaks at 2.35 T. The simulations of the carbon−chlorine residual dipolar coupling in both polymorphic forms reproduce all of the observed features in the spectra and are in excellent agreement at all three field strengths as shown in Figures 3 and 4. The actual isotropic chemical shifts obtained from simulating the MAS spectra are given in the δ_{CPMAS} column in Table 1.

Effect of Conformation and Intermolecular Interactions on the Quadrupolar Coupling. The parameters used for the simulations in Figures 3 and 4 are shown in Tables 2 and 3. The accuracy in the asymmetry parameter η is approximately 0.03. The asymmetries and quadrupolar coupling constants are comparable to quadrupolar coupling constants found for other six-membered aromatic systems with electronegative substituents.[32] The orientation of the EFG tensor relative to the molecular frame is only significant for the coupling to the carbons in β-position to the chlorine, since the *z*-axis is directed, as expected, along the C−Cl bond. The error in ϕ is about 20° for **Y-I** because of the small magnitude of the dipolar coupling to the carbons in β-position. The simulated spectra of **W-I** are insensitive to changes in the angle ϕ, since the asymmetry is small. The dipolar coupling constants obtained are smaller by 3.5% for **Y-I** and 2% for **W-I** than the dipolar coupling constants predicted from the X-ray diffraction data. However, it is known that dipolar coupling constants calculated from X-ray distances are 2−5% larger than the values determined experimentally by NMR.[42]

As discussed by Lucken,[32] the coupling constant χ and the asymmetry η are significantly influenced by the electronegativity of the neighboring group and the nature of the chemical bond. The conformational differences between the two polymorphs have a great effect on the electronic properties of the molecule. In **Y-I** the ester group is in plane with the aromatic ring allowing conjugation, resulting in a higher electronegativity of the aromatic system and therefore to a larger quadrupolar coupling. The larger asymmetry is observed due to the electron depletion of the lone-pair in the chlorine p-orbital perpendicular to the aromatic plane. Conversely, the large torsional angle between the ester group and the aromatic system in **W-I** prevents the mutual π-systems from overlapping, thereby reducing the electron depletion at the chlorine. The resulting electron distribution leads to a lower quadrupolar coupling constant and a lower asymmetry in **W-I** as observed.

The Towns and Dailey analysis can be used to calculate the fractional π-bond population ρ_π of the C−Cl bond from the quadrupolar coupling:

(42) Zilm, K. W.; Grant, D. M. *J. Am. Chem. Soc.* **1981**, *103*, 2913.

$$\rho_\pi = \frac{2}{3}\left|\frac{e^2Qq}{e^2Qq_o}\right| \cdot \eta$$

where $e^2Qq_o/h = 109.6$ MHz is the quadrupolar coupling of the chlorine atom.[32] For **W-I** and **Y-I** ρ_π is calculated to be 1.7 and 6.7%, respectively.[43]

Isotropic ^{13}C Chemical Shifts. The conformational differences of the two polymorphic forms result in substantial isotropic chemical shift differences ranging from 3.8 to 10.3 ppm for the aromatic carbons C_{OH}, C_{Cl} and C_i (Table 1, Figure 5). The isotropic chemical shifts of C_{O2} and C_{Me} on the other hand show only a small effect (<2.2 ppm) due to the changes in conformation. The isotropic chemical shifts in solution exhibit a strong solvent effect, and individual shifts in different solutions differ by several ppm. When the ^{13}C shifts in different solvents are compared to the CPMAS data of the two polymorphic forms, it is readily seen that solutions of **I** in the nonpolar solvents such as chloroform and benzene and **Y-I** have similar isotropic chemical shifts. Solutions of **I** in polar hydrogen-bond-forming solvents such as methanol and DMSO exhibit isotropic chemical shifts similar to those measured in **W-I**. This observation reveals similarities between the conformation of the two polymorphic forms and the conformations and hydrogen bond arrangements present in solution. In nonpolar solvents, where the solvent does not allow intermolecular hydrogen bonds, the planar conformation with an intramolecular hydrogen bond is lowest in energy. On the other hand, hydrogen-bond-forming solvents promote the formation of intermolecular hydrogen bonding between solvent and solute. Because of steric crowding in the aromatic plane, the conformation with a large torsional angle should then be favored, resulting in a conformation similar to **W-I**. A thorough interpretation of the isotropic chemical shifts in solution, however, would require equilibrium between several species that exceeds the scope of this investigation. Byrn et al[21] has already mentioned similar hydrogen-bond patterns in the different crystalline and solution species. However, the previous findings were based on spectroscopic data on different solutions and on the X-ray crystal structure.

^{13}C Chemical Shift Principal Values. The FIREMAT[14] experiment is a 2D solid-state NMR method that provides the isotropic spectrum in one dimension and the CSA information in the other dimension. Since the chlorine-coupled resonances are split into multiplets, a complication arises when the chemical shift principal values are determined from the FIREMAT dataset. For each peak of the multiplets a set of principal values is obtained. As already mentioned, doublet-like resonances are observed for C_{OH} and C_{Cl} in **W-I** and C_{Cl} in **Y-I** due to residual dipolar coupling. The averaged principal values for these resonances are obtained by averaging each component over the two obtained values. The situation is more complicated for the C_i position in **W-I**, where a triplet is observed. The simulation of the residual dipolar coupling to the chlorine shows that this triplet is due to a overlap of two doublet-like resonances resulting from two different ^{13}C positions, each of which represents one of the two molecules per unit cell in **W-I**. To obtain the principal shift values for the different molecules per unit cell both the high-field principal values and the low-field principal values are averaged with the center principal values (Table 1 and Figure 5).

The differences in the torsional angle of the ester group, the hydrogen bonding, and the change in bond length (especially the C−Cl bond) affect the conjugation for the entire aromatic

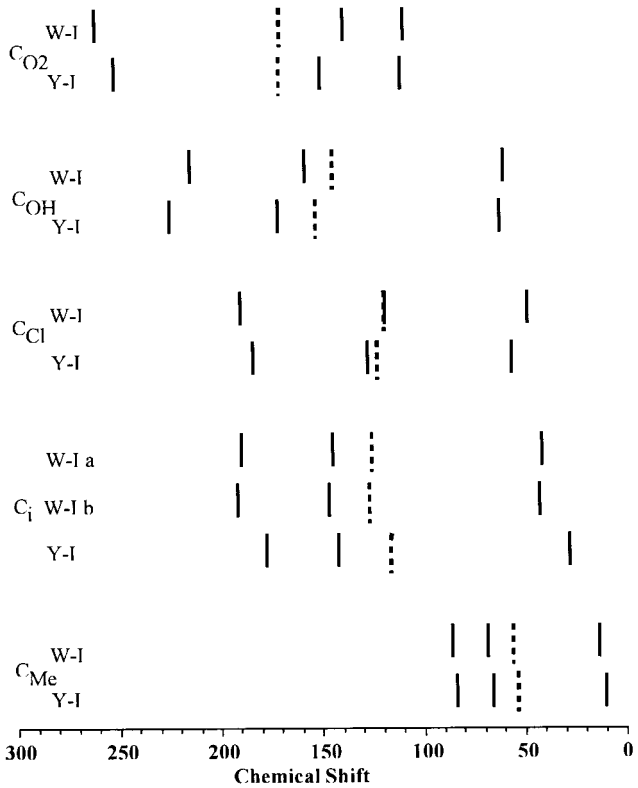

Figure 5. Experimental chemical shift principal values and isotropic chemical shifts for **W-I** and **Y-I**. Solid lines represent the chemical shift principal values and the isotropic chemical shifts are represented by dashed lines. The isotropic chemical shift and δ_{22} of C_{Cl} in **W-I** overlap.

π-system. Consequently, all chemical shift values are affected, as the chemical shift is a very sensitive probe of the local electronic environment. Exceptionally large shift differences up to 14 ppm between the two forms are observed for δ_{22} at the C_{OH} position and for δ_{33} at the C_i position. Even in the less sensitive methoxy-carbon shifts, differences of 2−3 ppm are measured. From Figure 5 it is readily seen that the conformational differences of the two polymorphic forms are better resolved by the chemical shift principal values than by the isotropic chemical shift alone. In particular, the substantial differences in the C_{O2} environment are not well characterized by the isotropic chemical shift, with a difference of only 1.3 ppm between **W-I** and **Y-I**. However, the δ_{11} and δ_{22} principal values differ by −9.3 and +11.1 ppm, respectively.

The effect of hydrogen bonding on the ^{13}C chemical shift principal values of CO_2H groups of amino acids has been previously studied.[44,45] It was found that the strength of the hydrogen bond affects the δ_{11} and δ_{22} chemical shift principal values, with a stronger hydrogen bond shifting δ_{11} to lower and δ_{22} to higher chemical shift values. The δ_{33} value is found to be unaffected by changes in hydrogen-bond strength. The δ_{33} values reported in the literature (av 109 ppm) agree with the δ_{33} values of C_{O2} determined for **W-I** and **Y-I**. Therefore, the lower δ_{11} and higher δ_{22} chemical shift for C_{O2} in **Y-I** may be explained by the shorter OC═O···H distance and stronger intramolecular hydrogen bond in **Y-I** than in **W-I**.

The strong hydrogen bond in **Y-I** also results in higher δ_{11} and δ_{22} values for C_{OH} than in **W-I**, whereas the δ_{33} is again unaffected by the difference in hydrogen bonding. However, a

(43) Bersohn, R. *J. Chem. Phys.* **1954**, *22*, 2078.

(44) Gu, Z.; Zambrano R.; McDermott, A. *J. Am. Chem. Soc.* **1994**, *116*, 6368.

(45) Facelli, J. C.; Gu, Z.; McDermott, A. *Mol. Phys.* **1995**, *86*, **4**, 865.

Table 4. Correlation between Experiment and Calculated Chemical Shift Principal Values

	W-I a		W-I b		Y-I		combined[a]	
	one molec.	three molec.	one molec.	three molec.	one molec.	three molec.	one molec.	three molec.
std. dev./ppm	8.2	6.0	8.6	5.9	5.7	4.5	7.3	5.3
slope	−0.9530	0.9832	−0.9624	−0.9890	−0.9595	−0.9951	−0.9583	−0.9891
intercept/ppm	183.7	185.9	183.7	186.0	183.0	188.5	183.5	186.8
R^2	0.9865	0.9931	0.9856	0.9934	0.9936	0.9962	0.9885	0.9941

[a] The experimental and theoretical values for all three structures are correlated together.

systematic study of the effect of hydrogen-bond strength on the chemical shift principal values of alcohol carbons is not available. It is difficult to attribute other differences in the chemical shift principal values to specific structural differences between the two polymorphic forms, because of the extensive conformational differences and the lack of systematic investigations of the effect of conformation on the chemical shift principal values.

The above analysis clearly shows that the chemical shift principal values are very useful for the investigation of polymorphism, as they provide a more accurate characterization of differences in conformation and intermolecular interactions such as hydrogen bonding than the isotropic chemical shifts. Investigating the chemical shift principal values provides complementary data to X-ray methods, especially when the difference between polymorphic forms constitutes of hydrogen bonding,

Chemical Shift Tensor Calculations. In Table 4 the slopes and intercepts as well as the standard deviation are given for the correlation of the various calculations with the experimental data. The slopes (−0.9530 to −0.9951), intercepts (183.0 to 188.5 ppm), and standard deviations (4.5 to 8.2 ppm) of the fits are close to those previously found for B3LYP D95**.[46,47] The intercepts compare favorably with the calculated shielding of methane at the same level of theory and basis set (192.4 ppm) when properly adjusted to the TMS scale by subtracting the 7 ppm difference between gas-phase methane and TMS resulting in an intercept of 185.4 ppm.[48] Figure 6 shows the correlation plot between the experimental principal shift values and the calculated shielding values using the B3LYP exchange functional on a single **W-I a**, **W-I b**, and **Y-I** molecule and on stacks of three molecules. In Table 5 the converted chemical shift principal values for the calculations on stacks of three molecules are given to allow comparison with the experimentally determined chemical shifts.

The agreement between experiment and theory is improved by increasing the size of the calculated system to a stack of three molecules (Table 4). The molecules were chosen to include the intermolecular hydrogen bonds in the case of **W-I**. For **Y-I** where there are only weak intermolecular interactions, the nearest neighboring molecules were chosen to obtain a similar molecular arrangement (Figure 1). The correlation and the standard deviation between experiment and calculated values for **W-I a** and **W-I b** are considerably improved when the calculations are done on a stack of three molecules. The correlation of the calculated data obtained on one molecule for **Y-I** already give a satisfactory correlation with the experimental data, and the improvement in going to the three-molecule stack is considerably smaller than for **W-I a** and **W-I b**. An improvement due to basis set superposition cannot account for the substantial better correlation observed for **W-I a** and **W-I b** when the calculations are done on stacks of molecules, as

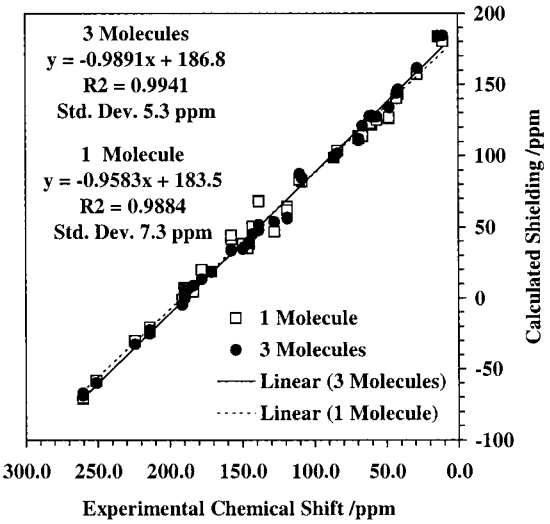

Figure 6. Correlation between calculated shielding principal values and experimental chemical shift principal values. The theoretical values are obtained with the B3LYP D95** method. The correlation is done on the experimental and theoretical values of **W-I a**, **W-I b**, and **Y-I** combined.

Table 5. Calculated Chemical Shift Tensor Principal Values for **W-I a**, **W-I b**, and **Y-1** Using the B3LYP D95** Method on a Stack of Three Molecules/ppm

	δ_{11}	δ_{22}	δ_{33}	δ_{iso}		δ_{11}	δ_{22}	δ_{33}	δ_{iso}
	C_{O2}					C_i			
W-I a	258.5	140.7	103.3	167.5	**W-I a**	187.3	150.2	40.7	126.1
W-I b	256.7	136.7	103.9	165.8	**W-I b**	193.8	150.3	43.3	129.1
Y-I	249.6	153.9	100.5	168.0	**Y-I**	175.5	143.3	25.5	114.8
	C_{OH}					C_{Me}			
W-I a	211.7	155.2	59.4	142.1	**W-I a**	88.5	75.8	2.9	55.7
W-I b	214.4	154.6	60.2	143.1	**W-I b**	88.3	76.9	2.5	55.9
Y-I	222.0	170.3	59.5	150.6	**Y-I**	86.2	66.5	2.4	51.7
	C_{Cl}								
W-I a	184.0	131.6	53.2	123.0					
W-I b	189.7	132.3	53.0	125.0					
Y-I	180.1	134.6	60.0	124.9					

typical basis set superposition errors only account for changes less than 2 ppm in the components.[49,50]

In Figure 7 the improvement in the B3LYP D95** results obtained by including the hydrogen bonding is shown graphically, allowing for a more refined discussion of the observed improvements. Comparison of the calculations done on isolated molecules and stacks of molecules reveals that substantial improvement of 5 to 16 ppm is achieved for those chemical shift principal values (δ_{11} and δ_{22} of C_{O2}) which are known to be affected by intermolecular hydrogen bonding as encountered in the white polymorphic form. In addition, an improvement of 7 and 10 ppm is achieved for the δ_{22} values of C_{OH} in **W-I a**

(46) Harper, J. K.; McGeorge, G.; Grant, D. M. *J. Am. Chem. Soc.* **1999**, *212*, 6488.

(47) Barich, D. H.; Orendt, A. M.; Pugmire, R. J.; Grant, D. M. *J. Phys. Chem.* A **2000**, *104*, 8290, and previous papers in series.

(48) Jameson, A. K.; Jameson, C. J.. *Chem. Phys. Lett.* **1987**, *134*, 461.

(49) Clementi, E.; Corongin, G.; Chakravorty, S. In *Modern Techniques in Computational Chemistry*; Clementi, E., Ed.; Escom: Leiden, 1990; p 343.

(50) Facelli, J. C. *Chem. Phys. Lett.* **2000**, *322*, 91.

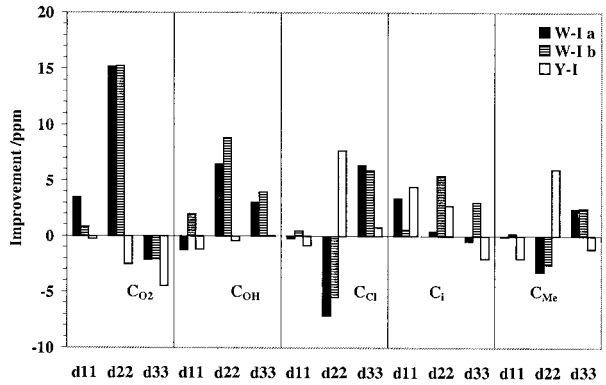

Figure 7. Improvement achieved when the system size is increased from a single molecule to a stack of three. The improvement is defined as: Improvement = |PV one molecule − PV experiment| − |PV three molecules − PV experiment|. PV one molecule: Chemical shift principal values obtained from B3LYP D95** calculations done on one molecule. PV three molecules: Chemical shift principal values obtained from B3LYP D95** calculations done on a stack of three molecules. PV experiment: Experimentally determined chemical shift principal values.

and **W-I b**, respectively. In the yellow polymorphic form, however, no significant improvements for the chemical shift principal values of any carbons, except the δ_{22} value of C_{Me}, is obtained with the addition of the neighboring molecules, implying that the intermolecular interactions are negligible.

The calculated shielding values of carbons adjacent to chlorine are also strongly affected by the size of the calculated system in both polymorphic forms, but the δ_{22} value of C_{Cl} in the white polymorph deteriorates recognizable. Considerably different quadrupolar coupling constants are obtained for the isolated and stacked molecules, indicating that the lattice substantially influences the polarizable chlorine electron cloud (Table 3). The systematic uncertainty in the experimental C_{Cl} chemical shift principal values, however, does not allow a highly refined interpretation.

The improvement in **W-I** is exceptional, because of the strong intermolecular interactions present. Hence, the agreement between calculated and experimental chemical shifts may be substantially improved by explicitly including strong intermolecular interactions in the calculations.[51−54]

EFG Tensor Calculations. The calculated tensors for **W-I** employing the B3LYP functional and a stack of three molecules show good agreement with the orientations and values found to give the best fit between simulation and recorded spectra (Table 3). The values calculated for **Y-I**, however, differ by a significant amount from the experimentally determined quadrupolar coupling constant and asymmetry. The agreement between experimental and theoretical data may be improved by a correlation. However, a reliable correlation on extensive experimental and theoretical data is only available for MP2 TZVP calculations,[55] which are not feasible on the relatively large stacks of three molecules of **I**.

The trends, however, observed for the differences between the two forms in the quadrupolar coupling are reproduced by the calculations for both the HF D95** and B3LYP D95** methods. The fact that the calculated EFG changes by about 0.4−0.6 MHz in χ_{zz} and by about 0.07−0.13 in η, when the calculations are done on stacks of molecule, suggests that lattice effects have a substantial effect on the EFG tensor and should not be neglected. The large differences for the orientation of the *x* and *y* principal axis with respect to the molecular frame for **W-I** for different levels of theory and different system sizes is due to the fact that the asymmetry is small and differences in theory and system size have, therefore, a significant effect on the orientation of the tensor. These differences, however, have a small impact on the observed spectra, because of the relatively small asymmetry.

Conclusions

The carbon isotropic chemical shift values and the chlorine electric field gradient (EFG) tensor information are extracted from the ^{13}C MAS spectra, and the principal values of the chemical shift tensors of the carbons are obtained from 2D FIREMAT experiments on two of the three known polymorphs of dimethyl-3,6-dichloro-2,5-dihydroxyterephthalate. These solid-state NMR parameters are shown to be very sensitive to the changes in geometry, electronic structure, and hydrogen bonding between the two polymorphs. The same data are obtained from quantum chemical calculations of the chemical shift and the EFG tensors. The ^{13}C MAS isotropic chemical shift values are compared to isotropic chemical shifts of solutions of dimethyl-3,6-dichloro-2,5-dihydroxyterephthalate in different solvents. When **I** is dissolved in nonpolar solvents, the isotropic chemical shifts are similar to those observed for **Y-I**. Solutions of **I** in polar hydrogen-bond-forming solvents have isotropic chemical shifts similar to the isotropic shifts of **W-I**.

Differences in the isotropic chemical shifts between the two polymorphs from 1 to 9 ppm are observed, with the largest differences found for the carbon of the aromatic ring. However, the differences in the individual chemical shift tensor components exhibit better structural sensitivity and are more specific when conformational differences are investigated. For the ester carbon, the isotropic chemical shift difference is only 1 ppm, while the differences in the δ_{11} and δ_{22} are each about 10 ppm, but in opposing directions. The difference in the chemical shift tensor principal values for this carbon between the two forms is well understood in terms of the hydrogen-bonding interaction that is much stronger in the white form.

The calculations of the chemical shift tensor were completed using the X-ray geometries with adjusted C−H distances on both isolated molecules and on stacks of three molecules chosen such that the intermolecular hydrogen bonding present in the white form was included. In going from a single molecule to the stack of three in the white form there was a significant improvement in agreement between theory and experiment. For the yellow form, in which there are no significant intermolecular interactions, the two results were fairly similar. More importantly, the improvement observed in the white form was found in those components of the ester carbon, which are known to be sensitive to hydrogen bonding, and the δ_{22} of the C_{OH} carbon.

Due to the presence of the chlorine atoms in this molecule a residual dipolar coupling between $^{35,37}Cl$ and the neighboring carbons is observed in the ^{13}C MAS spectra. The simulation of the MAS spectra of both polymorphic forms gives accurate isotropic chemical shift values, data on the EFG tensors of the chlorine and the dipolar coupling constants. Spectra were recorded at three different magnetic field strengths, and the spectral parameters were varied to achieve an excellent fit on

(51) Orendt, A. M.; Facelli, J. C.; Grant, D. M. *Chem. Phys. Lett.* **1999**, *302*, 499.
(52) Hu, J. Z.; Facelli, J. C.; Alderman, D. W.; Pugmire, R. J.; Grant, D. M. *J. Am. Chem. Soc.* **1998**, *120*, 9863.
(53) Facelli, J. C.; Pugmire, R. J.; Grant, D. M. *J. Am. Chem. Soc.* **1996**, *118*, 5488.
(54) de Dios, A. C.; Oldfield, E. *Solid State NMR* **1996**, *6*, 101.
(55) Palmer, M. H.; Blair-Fish, J. A. *Z. Naturforsch.* **1998**, *53a*, 370.

all three. The larger asymmetry found for the yellow polymorphic form can be explained by the small torsional angle between the ester group and the aromatic ring, resulting in a electron depletion in the chlorine lone-pair p-orbital perpendicular to the aromatic ring. The trends observed for the differences in the EFG tensor between the two polymorphic forms are also found in the quantum chemical calculation of the EFG tensor at the chlorine. However, the absolute agreement between calculations and experiment is only moderate and can certainly be improved by correlation between calculated experimental data, when more theoretical data at the level of theory used are available.

Acknowledgment. This research was supported by the Institute of General Medical Sciences, NIH, under Grant No. GM08521-39 and by the office of Basic Energy Sciences, DOE, under Grant No. DE-FG-94ER14452. An allocation of computer time from the Center for High Performance Computing at the University of Utah is gratefully acknowledged. CHPC's SGI Origin 2000 system is funded in part by the SGI Supercomputing and Visualization Center Grant.

JA003599B